

Measurements of the Magnetic Field Induced by a Turbulent Flow of Liquid Metal

M.D.Nomberg, E.J.Spence, R.D.Kendrick, and C.B.Forest
 Department of Physics
 University of Wisconsin-Madison
 1150 University Ave.
 Madison, WI 53706
 Dated: February 9, 2020)

Initial results from the Madison Dynamo Experiment provide details of the inductive response of a turbulent flow of liquid sodium to an applied magnetic field. The magnetic field is reconstructed from measurements both outside and within the flow. Differential rotation of the fluid generates a large mean toroidal magnetic field from an externally-generated axial field through the effect. Mean poloidal magnetic flux is expelled from the fluid by the poloidal flow. Small-scale, time-varying magnetic field structures are generated by turbulence in the flow. The resulting magnetic power spectrum exhibits the characteristic power-law scalings expected from Kolmogorov-like turbulence with an apparent knee at the resistive dissipation scale. Large-scale velocity fluctuations create dynamical flow profiles that generate intermittent bursts of non-axisymmetric magnetic fields indicating that the transition from damped magnetic fields to growing magnetic fields is not smooth for a turbulent flow.

PACS numbers: 47.65.+a, 91.25.Cw

Keywords: magnetohydrodynamics, MHD, dynamo, turbulence

I. BACKGROUND

The generation of magnetic fields by flowing electrically-conducting fluids is a long-standing problem in plasma physics, astrophysics, and geophysics. Of particular interest is the role of turbulence in either supporting or suppressing magnetic fields. Dynamos have been created in the laboratory by linking the development of turbulence to scales much smaller than the device size [1, 2]. This scale separation inhibits dynamos due to large-scale turbulence which can be important in astrophysical contexts, especially for the transition a flow undergoes to produce a growing magnetic field. The Madison Dynamo Experiment was built to characterize these dynamos.

The experiment, shown in Fig.1, uses two impellers to generate a double-vortex flow of liquid sodium in a 1m diameter spherical vessel. Liquid sodium is used due to its high conductivity. The choice of a spherical geometry is motivated by the computational work of Dudley and James which demonstrated that simple time-stationary vortices can self-excite at relatively low speeds [3]. The flow has been measured in hydrodynamic experiments and is predicted by laminar dynamo theory to generate a transient magnetic field [4] by a slow-dynamo mechanism that stretches and twists magnetic field lines to regenerate the initial seed field [5]. Due to the low Prandtl number of liquid sodium ($Pr = 10^5$) and the large magnetic Reynolds numbers required for spontaneous field growth ($Re_{crit} = 10^8$), the flows required for a dynamo are extremely turbulent ($Re = 10^7$). These types of flows are also studied in experiments at

Maryland [6] and Cadarache [7]. The open geometry of these experiments provides the opportunity to study the role of large-scale turbulence in magnetic field generation.

The purpose of this correspondence is to provide a description of the Madison experiment and to report the initial measurements of the magnetic field induced by the flowing liquid metal. The theory of laminar kinematic dynamos and hydrodynamic measurements of the flow are reviewed in Sec. II. The experimental apparatus and its diagnostics are described in Sec. III. Measurements of the mean magnetic field induced when an external magnetic field is applied to the turbulent flow are compared to predictions from the laminar theory in Sec. IV. Measurements of the magnetic field fluctuations reveal intermittent bursts of magnetic fields and frequency spectra with power-law scaling which are explained in Sec. V. It is found that turbulence in the flow not only creates small-scale magnetic field structures, but also produces large-scale intermittent behavior.

II. THE KINEMATIC DYNAMO

A. Theory

The evolution of the magnetic and velocity fields in an incompressible conducting fluid is governed by the magnetic induction equation and Navier-Stokes equation:

$$\frac{\partial \mathbf{B}}{\partial t} = \mathbf{r} \cdot \mathbf{v} \times \mathbf{B} + \frac{1}{\mu_0} \mathbf{r} \cdot \nabla \mathbf{B} \quad (1)$$

$$\frac{d\mathbf{v}}{dt} = \mathbf{J} \times \mathbf{B} - \mathbf{r} \cdot \mathbf{p} + \mathbf{r}^2 \mathbf{v}; \quad (2)$$

where μ_0 is the vacuum magnetic permeability, \mathbf{r} is the fluid conductivity, \mathbf{p} is the fluid density, and \mathbf{v} is

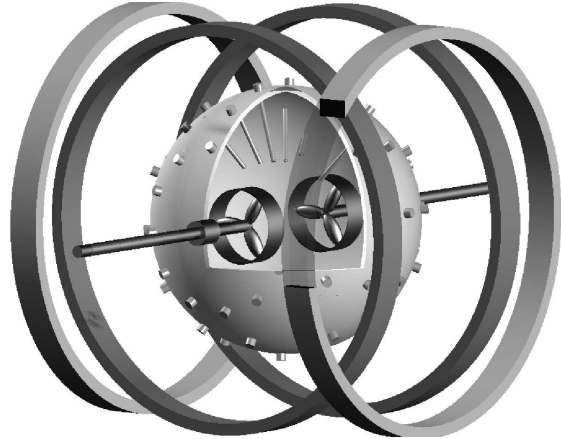
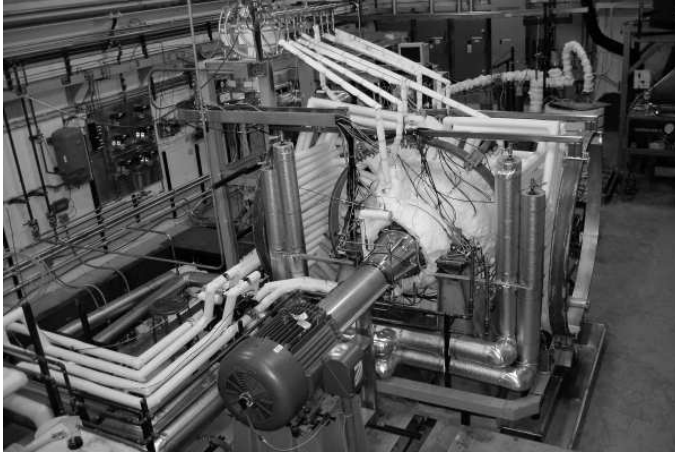


FIG. 1: Photograph and schematic of the Madison Dynamo Experiment. The sphere is 1 meter in diameter. It is filled with 105{110 C liquid sodium and a flow is created by two counter-rotating impellers. Two sets of coils, one coaxial and one transverse to the drive shafts, are used to apply various magnetic field configurations. The magnetic field induced by the flow is measured using Hall effect sensors both on the surface of the sphere and within tubes that extend into the flow.

the viscosity. The time scale for magnetic diffusion is $\tau_0 = a^2/\eta$ where a is a characteristic size of the system. Recast in dimensionless units the induction equation becomes

$$\frac{\partial \mathbf{B}}{\partial t} = Rm \mathbf{r} \cdot \nabla \mathbf{B} + \mathbf{r}^2 \mathbf{B} \quad (3)$$

where the magnetic Reynolds number $Rm = \eta_0 a v_0$ is a measure of the rate of advection compared to the rate of diffusion (v_0 is a characteristic velocity). The relative importance of the Lorentz force in the flow dynamics is given by the interaction parameter $N = a B_0^2/v_0$ where B_0 is a characteristic field strength. For a kinematic dynamo $N \gg 1$ so that the velocity field evolves independently of the magnetic field. For a stationary flow, the induction equation becomes linear and can be solved by expanding \mathbf{B} as

$$\mathbf{B}(\mathbf{r}; t) = \sum_i \mathbf{B}_i(\mathbf{r}) e^{i\omega_i t}; \quad (4)$$

where ω_i are the growth rates of the magnetic eigenmodes $\mathbf{B}_i(\mathbf{r})$. A dynamo is produced when there is at least one eigenvalue with a positive real growth rate.

A fundamental requirement for a flow to produce a dynamo is sufficiently fast flow speed so that the advection of the magnetic field overcomes ohmic dissipation [8]. There is a minimum magnetic Reynolds number Rm_{crit} below which resistive diffusion dominates the evolution of the field. One measure of how effectively the flow amplifies the magnetic field is the ratio of the magnitude of the induced field to the magnitude of the initial seed field; this ratio is defined as the gain. As $Rm \rightarrow Rm_{crit}$, the gain increases indicating stronger amplification of the induced field.

A second fundamental requirement for a flow to produce a dynamo is the correct geometry for producing

feedback | the induced field must regenerate the initial seed field. Hence, the feedback of the flow can be quantified by measuring the orientation of the induced field relative to the initial field. The magnetic fields induced in the Madison Dynamo Experiment are characterized in terms of the gain and feedback to understand the mechanism which produces a dynamo.

B. Experimental flow modeling

Although the impeller-generated flow in the experiment is turbulent, the mean flow can be approximated by a laminar model. Flows in a spherical geometry are most easily modeled by the Bullard and Gellman formalism where the velocity field is described by a spherical harmonic expansion of toroidal and poloidal stream functions [9]

$$\mathbf{V}(\mathbf{r}; \theta, \phi) = \sum_{m=0}^{\infty} \sum_{i=0}^m \left[\frac{r}{r-h} \mathbf{s}_{im}(\mathbf{r}) \mathbf{Y}_m^m(\theta, \phi) \hat{\mathbf{r}} \right] + \frac{h}{r} \mathbf{t}_{im}(\mathbf{r}) \mathbf{Y}_m^m(\theta, \phi) \hat{\mathbf{r}} \quad (5)$$

and the magnetic field is described by an expansion of flux functions

$$\mathbf{B}(\mathbf{r}; \theta, \phi) = \sum_{m=0}^{\infty} \sum_{i=0}^m \left[\frac{r}{r-h} \mathbf{s}_{im}(\mathbf{r}) \mathbf{Y}_m^m(\theta, \phi) \hat{\mathbf{r}} \right] + \frac{h}{r} \mathbf{T}_{im}(\mathbf{r}) \mathbf{Y}_m^m(\theta, \phi) \hat{\mathbf{r}} \quad (6)$$

The experimental flow is axisymmetric and is composed primarily of the $t_{2,0}$ and $s_{2,0}$ terms. Hence, it is called a t_2s_2 flow.

The velocity field depicted in Fig. 2(a) is determined from Laser Doppler Velocimetry (LDV) measurements

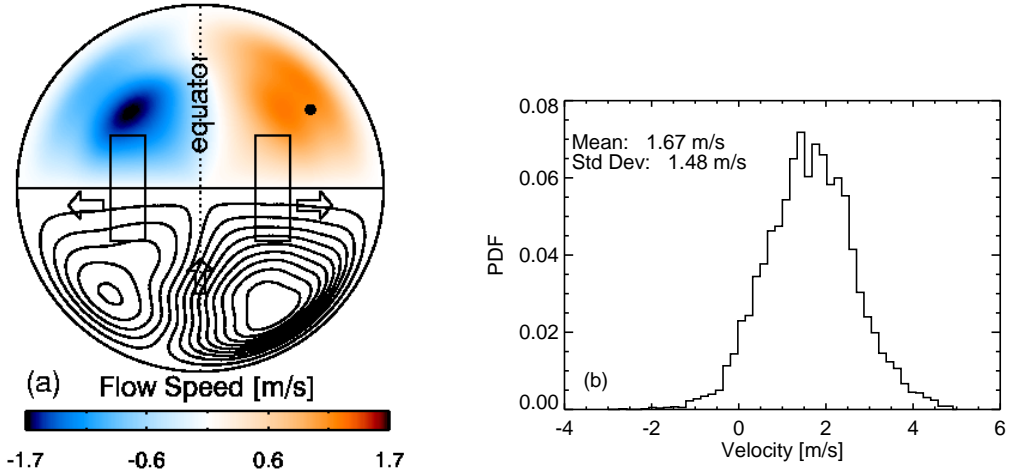


FIG . 2: (a) Velocity field pro les fitted to LDV measurements of water ows generated by impellers identical to those used in the sodium experiment. The impeller rotation rate is 15 Hz corresponding to $R_m = 90$ based on impeller tip speed. The toroidal ow is shown in the upper hemisphere and poloidal stream lines are shown in the lower hemisphere. The ow is directed inward at the equator and outward at the poles. The two rectangles represent the location of the impellers. The asymmetry across the equator is due to a slight difference in the impeller rotation rates which creates the odd ow harmonics. (b) The probability distribution function for an LDV measurement of the toroidal velocity in the water model of the sodium experiment. The measurement location is shown as the dot in (a).

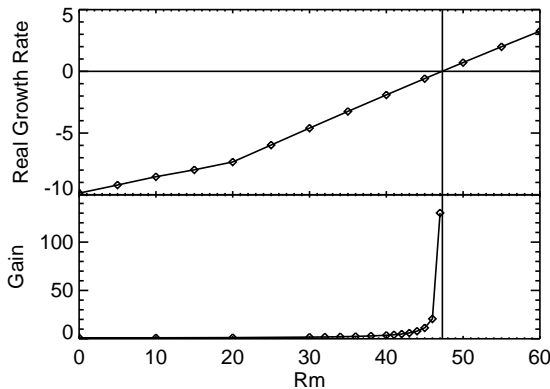


FIG . 3: The predicted growth rate of the dominant eigenmode versus R_m as determined by an eigenvalue stability analysis of an optimized model of the ow. Also shown is the gain defined as the ratio of magnitudes of the transverse eld induced by the ow and the initial transverse dipole eld. The amplification of magnetic ux grows as the ow reaches $R_m \text{ crit} = 47$.

performed in an identical-scale water model of the sodium experiment. Liquid sodium at 105 C has the same kinematic viscosity and density as water at 40 C, so the ow measured in the water model corresponds to the sodium ow. Since the ow is turbulent, these profiles are only realized in a mean sense. Fig.2 (b) shows the probability distribution function for an LDV measurement. The actual ow profiles are dynamic, implying that the eigenmode growth rate fluctuates on the time scale of the ow evolution. The induced eld thus ex-

hibits transient behavior, especially for ows near $R_m \text{ crit}$. The auto-correlation time of the LDV measurements of the ow is $\tau_c = 60 - 20$ ms which serves as an estimate of the time scale for changes in the ow profile.

An eigenmode analysis of an optimized version of the hydrodynamic ow suggests that a magnetic eld should be generated for $R_m = 47$ as seen in Fig.3. The structure of the magnetic eigenmode with the largest growth rate for the t2s2 ow is dominated by the $S_{1,1}$ term in the expansion of Eq.6 corresponding to a dipole eld oriented perpendicular to the axis of symmetry of the ow (note the eld lines in the first panel of Fig.4). The generated eld breaks the system's axisymmetry, thereby satisfying Cowling's theorem [8].

The physical mechanism of the gain and feedback for the t2s2 ow is demonstrated by following the evolution of a eld line in the frozen-ux approximation (the diffusion term in Eq.3 is neglected). In Fig.4, two eld lines parallel to the equatorial plane are stretched to the poles (located where the drive shafts enter the sphere) by the poloidal ow and twisted by the toroidal ow back into their original direction. The induced eld enhances the initial seed eld thereby increasing its magnetic ux. This process continues as tension in the eld lines is relieved through magnetic reconnection due to resistive diffusion. Once the magnetic eld becomes sufficiently strong, the interaction parameter becomes large. The Lorentz force creates a torque on the ow, referred to as the back reaction, which presumably halts the eld growth.

The linear analysis above may be inadequate for describing the experiment since turbulence also induces magnetic elds. Eddies in the ow distort the magnetic

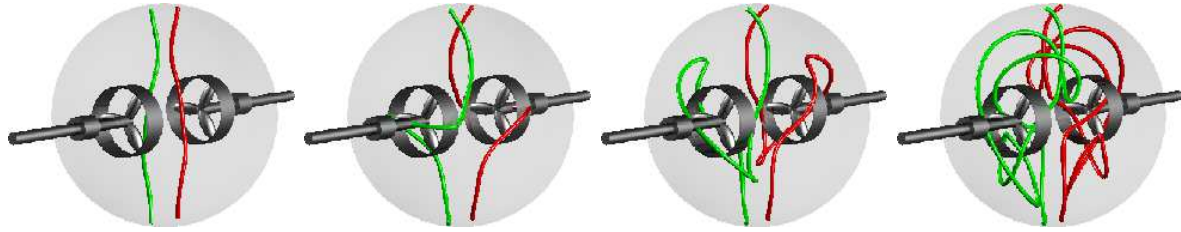


FIG. 4: The mechanism of field generation in a laminar double-vortex flow is modeled in the frozen flux limit ($R_m \neq 1$). A field line directed through the equator is stretched by the poloidal flow towards the pole and then twisted back onto itself by the toroidal flow.

eld creating small-scale magnetic field structures which can affect the large-scale induced field. Mean field theory suggests that velocity field fluctuations can enhance the resistivity of the fluid by effectively increasing the rate of diffusion (the α effect) [10], generate large-scale currents through helical fluid motion (the α effect) [11], and reduce the magnetic field within the flow due to inhomogeneities in the magnitude of turbulent fluctuations (the α effect) [12]. The usual assumptions of homogeneous, isotropic turbulence and scale separation of fluctuations from the mean flow are not satisfied in the experiment and so the effects described are only used for conceptual understanding.

III. DESCRIPTION OF THE EXPERIMENT

The experiments are performed in a 1 m diameter, 1 cm thick, stainless steel sphere shown in Fig. 1. Liquid sodium is transferred pneumatically from a storage vessel, located in a vault beneath the floor, to the sphere using pressurized argon. The sodium fills the sphere from the bottom until the liquid level rises to an expansion tank connected to the top of the sphere. The expansion tank accommodates changes in the volume of the sodium due to variation in temperature. The weight of the sodium in the storage vessel is monitored during the transfer to determine the liquid level in the sphere. Electrical contact switches in the expansion tank provide a redundant means of determining the sodium fill level.

The conductivity of liquid sodium varies with temperature. It has a maximum value of 1.5×10^7 (m)⁻¹ near the freezing point of sodium (98 °C) and decreases by about 4% for every 10 °C. Since $R_m \propto 1/T$, the sphere is kept at a temperature of 105–110 °C to optimize R_m without freezing the sodium. The sphere's temperature is maintained by a heat exchange system which runs heat-transfer oil through a series of copper tubes on the sphere's surface. The system provides 12 kW of heating and 75 kW of cooling to the oil. Kaowool insulation reduces the sphere's ambient heat loss. The heat introduced to the sodium by the rotating impellers is removed through the surface of the sphere by the heat exchange system.

Two 30.48 cm diameter impellers generate the flow. They are driven by 75 kW motors controlled by vari-

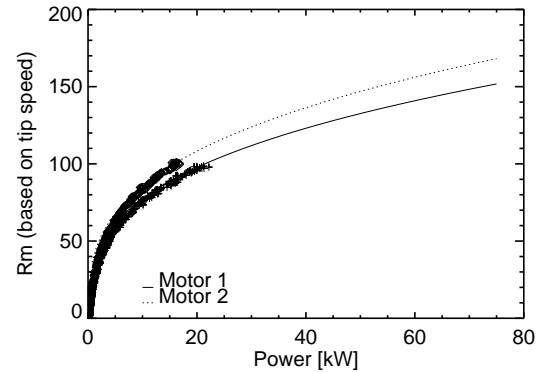


FIG. 5: The motor power follows the characteristic cubic relationship with the impeller rotation rate which is proportional to R_m . The curve is extrapolated to the maximum motor power available, yielding $R_{m_{max}} = 150$:

able frequency drives (VFDs). The motors rotate the impellers at rates from 3–30 Hz (R_m is between 18–180). Since R_m depends on flow geometry, the impellers have been modified to produce the desired flow [5]: Kort nozzles limit the radial thrust and fins on the exterior of the nozzles increase the mean toroidal flow. The magnetic Reynolds number R_m is approximated using the rotation rate of the impellers measured by digital encoders. Although convenient, this estimate is generous in that the speed of the impeller tip is much larger than that of the bulk flow. The VFDs record torque and power information. The motor power follows a cubic relationship with rotation rate as shown in Fig. 5. The back reaction due to magnetic field generation will increase the power required to drive the impellers thereby modifying the motor power curve.

At atmospheric pressure, the impellers cause cavitation by creating a rapid drop in the local pressure near the impeller blades, forming bubbles in the fluid. When the bubbles collapse against the blades, they emit ultrasonic noise which is monitored by an ultrasonic transducer mounted to the sphere. Since these bubbles disrupt the flow through the impellers, the cavitation must be suppressed; this is accomplished by pressurizing the sphere with argon gas. The required pressurization is

determined empirically by increasing the sphere pressure until the ultrasonic noise is minimized. For example, to operate at a rotation rate of 20 Hz the sphere must be pressurized to 550 kPa (80 psi).

Two sets of coils generate magnetic fields used to study the induction effects of the flow. One set is coaxial with the drive shafts, the other orthogonal, as shown in Fig. 1. A DC power supply provides the coils with 600 A to generate fields up to 100 G. The coils can produce dipole, quadrupole, transverse dipole, and transverse quadrupole field configurations. For flow speeds of 10 m/s, the interaction parameter is $N = 10^3$ hence the magnetic field is advected passively by the flow.

The magnetic field is measured using Hall effect probes (Analog Devices AD22151 Linear Output Magnetic Field Sensors) on integrated circuits with internal temperature compensation. The probes saturate at 200 G and are low-pass filtered to match the 1 kHz skin-effect frequency of the stainless steel sphere. Probes are positioned on a grid on the surface of the sphere capable of resolving spherical harmonics modes up to a polar order of 7 and an azimuthal order of 5. Linear arrays of probes in stainless steel tubes are inserted radially into the sphere and are oriented to measure either axial or toroidal magnetic fields. Data from the magnetic probes is sampled by 16-bit digitizers on PC-based data acquisition cards at a rate of 1 kHz per channel. The stainless steel tubes encasing the internal sensor arrays vibrate when the impellers are driven at rotation rates above 15 Hz ($R_m = 90$). The amplitude of the vibrations increases with flow speed so experiments are limited to the lower rotation rates to prevent damaging the tubes and risking a breach. A comparison of data from experiments before the internal arrays were installed with data from experiments with the tubes indicates that the disturbance in the flow due to the tubes has negligible effect on the large-scale induced magnetic field. Future experiments will be performed without the internal sensor arrays to reach higher rotation rates.

IV. MAGNETIC FIELD MEASUREMENTS

A. Reconstruction of the mean magnetic field

The induction effects are studied by applying an axial magnetic field to both flowing and stationary sodium and comparing the measured fields. The flow's differential rotation wraps the field lines around the drive shaft axis to produce a toroidal magnetic field through the so-called !-effect, as seen in Fig. 6(a). The contour plot is generated by fitting the coefficients of the harmonic expansion in Eq. 6 to toroidal field measurements (up to order $' = 3$). The !-effect is very efficient at amplifying the magnetic field; measurements of the toroidal magnetic field shown in Fig. 6(b) indicate that the induced toroidal field increases with R_m and is larger than the applied field for $R_m = 120$. In contrast, Fig. 6 shows that the axial magnetic field in the equatorial plane is halved due to

expulsion from the intense shear layer between the two large flow cells.

The mean field structure shown in Fig. 6(a) is obtained by an averaging procedure which calculates the peak of the histogram of magnetic field measurements from each probe. This technique is necessary since some of the probes have non-Gaussian statistics (discussed in Sec. V). The resulting mean field is predominantly due to odd harmonics in accordance with the selection rules governing the interaction terms of the induction equation [9]. The presence of small even harmonics could be an indication that the flow is asymmetric across the equator due to an imbalance of the impeller rotation rates or possibly a turbulent EMF.

The magnetic field outside the sphere is reconstructed from the field harmonics calculated from the surface array measurements. The poloidal flux lines are shown in Fig. 6(a). Since the Hall probes on the surface of the sphere lie outside regions containing currents, the measured field can be described in terms of a spherical harmonic expansion of the vacuum field potential

$$(r; \theta; \phi) = \sum_{m=0}^{\infty} C_{,m} r^m \cos(m\phi) + \sum_{m=0}^{\infty} D_{,m} r^m \sin(m\phi) Y_m^m(\theta; \phi); \quad (7)$$

where $B = r$. The $C_{,m}$ terms are due to currents in the external field coils whereas the $D_{,m}$ terms are due to currents in the flow. The field can be separated into applied and induced fields whose radial components are

$$B_{\text{applied}} = \sum_{m=0}^{\infty} C_{,m} r^{m+1} Y_m^m(\theta; \phi); \quad (8)$$

$$B_{\text{induced}} = \sum_{m=0}^{\infty} D_{,m} \frac{r^{m+2}}{r^{+2}} (m+1) Y_m^m(\theta; \phi); \quad (9)$$

The external measured magnetic field can be completely described in terms of these expansion coefficients. To determine the coefficients for a given set of magnetic field measurements, a design matrix A_{ij} is constructed which satisfies

$$B_i = A_{ij} D_j \quad (10)$$

where B_i is an array of measurements of the induced field and D_j is the array of expansion coefficients in (9). The coefficients are obtained by matrix inversion using Singular Value Decomposition [13] to solve $D_j = (A_{ij})^{-1} B_i$. Time series measurements from several probes are shown in Fig. 7(a) along with plots of the computed axisymmetric modes at $\theta = 0$ in Fig. 7(b). The dipole component of the induced magnetic field grows non-linearly with R_m and cannot be explained by induction effects from the mean flow. The dipole response results from a turbulent EMF generated by correlated turbulent fluctuations in the flow [14].

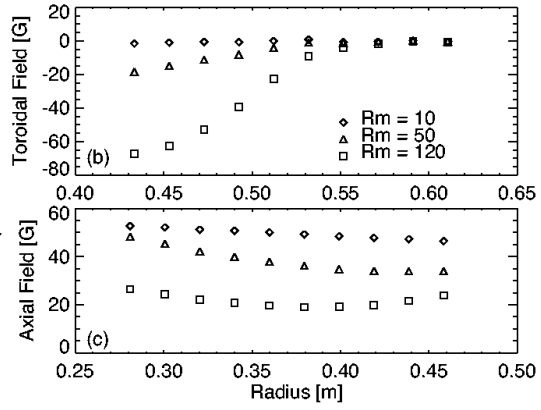
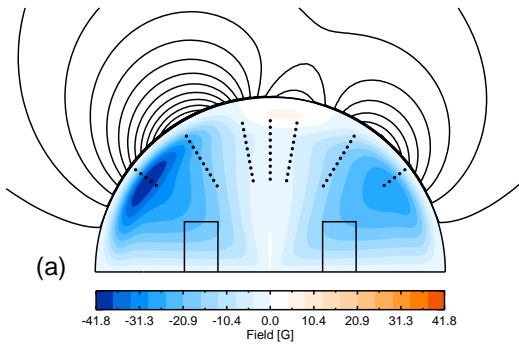


FIG. 6: (a) A plot of the toroidal magnetic field produced by the flow when a 60 G axial field is applied to a t2s2 flow with $R_m = 100$. The contours are calculated by fitting the expected T_{exp} profiles to measurements of the internal toroidal field. The dots indicate the position of the Hall probes. External field lines are shown based on a vacuum-field expansion fit to measurements from the surface probe array. (b) Toroidal magnetic field measurements near a pole and (c) axial magnetic field measurements in the equatorial plane for various R_m .

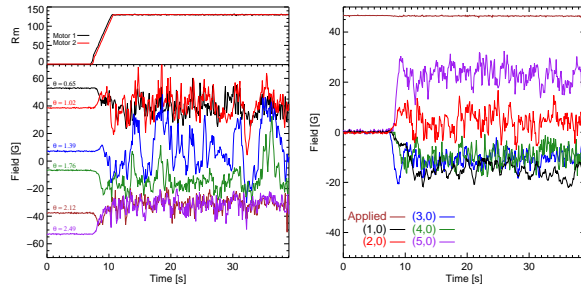


FIG. 7: (a) Time series measurements of the magnetic field at several positions on the surface of the sphere. (b) Time series plots of the axisymmetric modes evaluated at $\theta = 0$.

B. Measuring gain with a transverse applied field

The proximity of the flow to magnetic self-excitation is studied by applying a magnetic field perpendicular to the drive shaft axis. Recall from Sec. II that the anticipated structure of the magnetic field generated by the dynamo is a dipole oriented in this direction. Fig. 3(b) suggests that such a field should be amplified by the flow. The level of amplification depends both on the magnitude of the induced field and on its orientation. Therefore the gain is defined as

$$\text{gain} = \frac{B_{\text{induced}} \cos \phi + B_{\text{applied}}}{B_{\text{applied}}} \quad (11)$$

where the field magnitudes are calculated for the $\ell = 1, m = 1$ expansion term in Eq. 9 and ϕ is the azimuthal phase difference between the applied and induced fields. The gain is less than one if the induced field is antiparallel to the applied field, indicating attenuation, and is greater than one if the fields are in phase. The gain is determined from measurements of the induced magnetic field and is shown to increase with R_m in Fig. 8(a). Fig. 8(b) shows

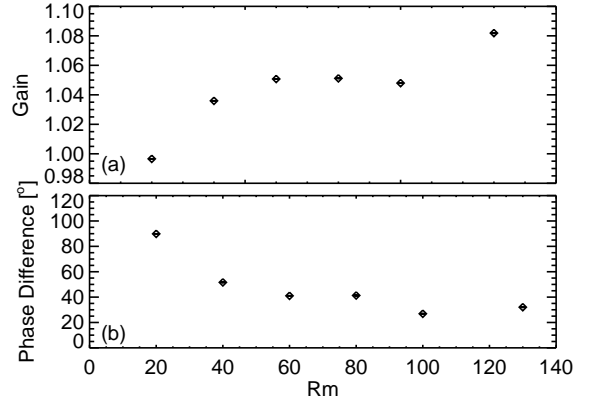


FIG. 8: (a) Amplification of a magnetic field applied perpendicular to the drive shaft axis as a function of R_m . Gain is defined in Eq. 11. (b) Phase angle difference between the induced transverse dipole moment and the applied field.

that the induced field is out of phase with the applied field at low R_m and in phase as R_m increases. These gain and phase angle measurements will be used to optimize the flow profiles in the sodium experiment.

V. PROPERTIES OF MHD TURBULENCE

The preceding analysis documents the large-scale induced mean field. Since the flow is turbulent and the magnetic field relatively weak, eddies can twist and stretch field lines at many scales. While smaller eddies are advected by the mean flow, larger eddies distort the large-scale flow itself causing intermittent behavior in the induced field. Fig. 9 shows signals from two Hall probes on the surface of the sphere and their probability distribution functions (PDFs). In addition to random fluctuations

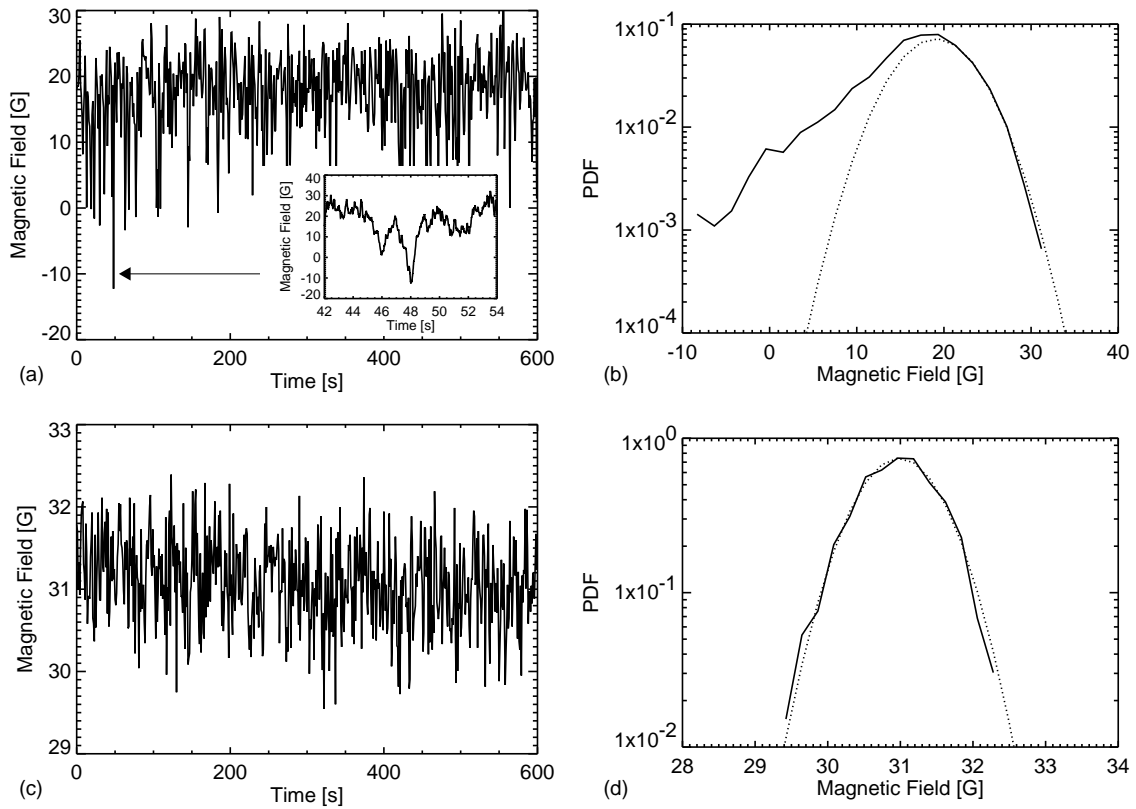


FIG . 9: (a) Measurement from a single Hall probe on the surface of the sphere near the equator and (b) its probability distribution. The impeller rotation rate for this example is 16.7 Hz ($R_m = 100$) and a 60 G dipole field is applied. A Gaussian fit to the right side of the distribution is shown (dotted line) to illustrate the asymmetry. The time series for a probe near the drive shaft axis (c) with its probability distribution (d) is shown for comparison.

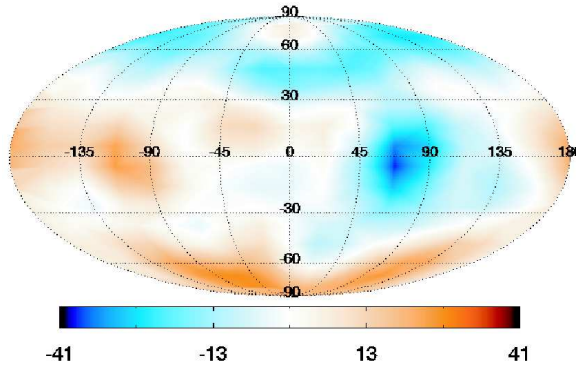


FIG . 10: The mode structure of a burst corresponds to a dipole field aligned perpendicular to the drive shaft axis (the axis of rotation is vertical).

ations with a Gaussian distribution, the Hall probe in Fig.9(a) has large-amplitude bursts which skew its PDF shown in Fig.9(b). The time average of the signal for this probe is therefore not the most-probable value of the field. The probe shown in Fig 9(c), however, has nor-

mal statistics. Examination of the structure of the magnetic field during the bursts reveals a strong mode shown in Fig.10. The large-scale turbulent flow thus induces an axisymmetric field on average punctuated by intermittent bursts that break the symmetry.

Eddies at the smaller scales create structure in the magnetic field down to the viscous dissipation scale [15]. This structure is evident in the spatial spectrum in Fig.11. The $k^{5/3}$ scaling corresponds to the weak-field approximation in which the induced field is balanced by the advection term in the induction equation [7, 16]. The magnetic field can be described in terms of a mean and a fluctuating part $B = \bar{B} + B_0$. At small scales, the magnetic field fluctuates on the diffusive time scale, thus

$$\frac{\partial \bar{B}}{\partial t} = -\frac{1}{0} r^2 \bar{B} : \quad (12)$$

Expanding \bar{B} and \bar{v} in terms of their Fourier components yields $\bar{v} = k^2 = \bar{v}_0 = k^2 v_0 a = R_m$ where a is a characteristic length. Assuming all fluctuations are due to the advection of spatial variations in the field, the dispersion relation becomes $\bar{v}(k) = v_0 k$. Resistive diffusion becomes important at the scale corresponding to

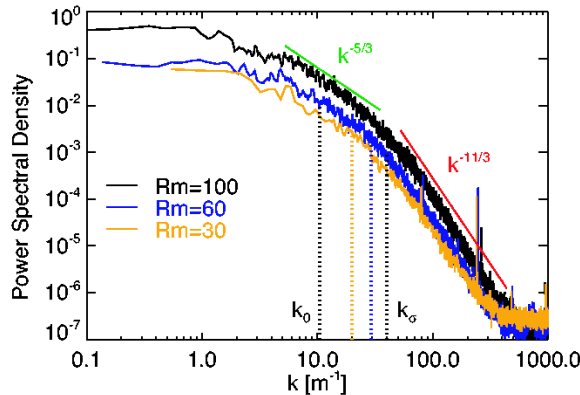


FIG. 11: Spatial spectrum constructed from the frequency response of a Hall probe inside the sphere (just above the impeller near the toroidal maximum in Fig.6). Fluctuations are assumed to be due to convection of spatial variations in the field. The dispersion relation is $\omega = kv_0$ where v_0 is determined from velocity measurements in the water model of the sodium experiment.

Rm	v_0 [m/s]	k [m⁻¹]
30	0.39	20
60	0.78	29
100	1.2	40

TABLE I: The resistive dissipation scale determined from the spatial spectrum in Fig.11. The velocity is measured in the water model of the experiment at the probe's position.

$k = v_0 / Rm = a$. At scales $k \ll k_0$, the dissipation term is small. Thus, magnetic fluctuations are due to advection of the mean field by velocity fluctuations and so

$$i! B(k) = ik \cdot \vec{v}(k) \cdot B_0 i. \quad (13)$$

Assuming homogeneous and isotropic turbulence, the power spectrum for the magnetic fluctuations is given by $B^2(k) = B_0^2 (k!)^2 \epsilon^2(k)$. Again, assuming the fluctuations are due to convection of spatial structures yields $B^2(k) = B_0^2 \epsilon^2(k) = v_0^2$. For Kolmogorov-type turbulence, $\epsilon^2(k) / k^{5/3}$ and so the magnetic power spectrum $E_M(k) / k^{5/3}$. For $k \ll k_0$ the advection and di-

sipation term becomes comparable and so

$$r \cdot \epsilon \cdot B_0 = \frac{1}{0} r^2 B \quad (14)$$

The magnetic power spectrum is then $B^2 = k^2 B_0^2 \epsilon^2 = v_0^2$. For Kolmogorov turbulence, $B^2 / k^{11/3}$ in the resistive dissipation range.

The dissipation scale is evident from the knee in the wave number spectrum of Fig.11. The spatial spectrum is constructed from the power spectrum of a Hall probe which measures the toroidal field just above one of the impellers. The results are summarized in Tab. I showing that k_0 increases with Rm . Consequently, the magnetic field gains structure at smaller scales as Rm increases, down to scale sizes of $\lambda = 2 \pi k_0 = 16 \text{ cm}$ at $Rm = 100$. A magnetic Reynolds number for the turbulent part of the flow can be constructed assuming that $k = Rm_{\text{turb}} k_0$. Using the values in Tab. I, it can be shown that $Rm_{\text{turb}} = 0.2 Rm_{\text{tip}}$ where Rm_{tip} is based on the tip speed of the impeller. This relation implies that the turbulent eddies produced by the mean flow are smaller and slower than the injection-scale eddies and hence the dissipation scale is only about one decade smaller than the injection scale rather than the two decades expected for a flow with $Rm = 100$.

VI. CONCLUSION

The magnetic field induced by a turbulent flow of liquid sodium demonstrates flux expulsion and the effect as anticipated for a laminar flow. The flow generated in the experiment induces a field that provides the gain and feedback necessary for a dynamo. Power spectrum measurements show that the resistive dissipation scale is proportional to Rm . Since turbulence is allowed to develop to the large scales, the flow processes are dynamical and excite intermittent bursts of symmetry-breaking fields. Consequently, as a flow nears Rm_{crit} , the transition to a dynamo is expected to be intermittent rather than smooth.

The authors would like to acknowledge the generous financial support for this project from the Department of Energy, the National Science Foundation, the Packard and Sloan Foundations, and the Research Corporation.

[1] R. Stieglitz and U. Müller, *Phys. Fluids* 13, 561 (2001), URL <http://link.aip.org/link/?PHF/13/561/1>.

[2] A. Gailitis, O. Lielausis, S. Dementev, E. Platnickis, A. Cifersons, G. Gerbeth, T. Gundrum, F. Stefani, M. Christen, H. Hanel, et al., *Phys. Rev. Lett.* 84, 4365 (2000), URL <http://link.aps.org/abstract/PRL/v84/p4365>.

[3] M. L. Dudley and R. W. James, *Proc. R. Soc. London, Ser. A* 425, 407 (1989).

[4] R. O'Connell, R. Kendrick, M. Nornberg, E. Spence, A. Bayliss, and C. Forest, in *Dynamo and Dynamos*, a Mathematical Challenge, edited by P. Chossat, D. Ambroster, and I. Oprea, NATO Science Programme (Kluwer Academic Publishers, 2000), vol. 26 of *NATO Science Series II, Mathematics, Physics and Chemistry*, pp. 59–66.

[5] C. Forest, R. Bayliss, R. Kendrick, M. Nornberg, R. O'Connell, and E. Spence, *Magnetohydrodynamics*

38, 107 (2002).

[6] D . Lathrop, W . Shew, and D . Sisan, *Plasma Physics and Controlled Fusion* 43, A151 (2001).

[7] M . Bourgoin, L . Marie, F . Petrelis, C . Gasquet, A . G uigon, J.-B . Luciani, M . M oulin, F . N am er, J . Bur-
guete, A . Chi audel, et al., *Phys. Fluids* 14, 3046 (2002),
URL <http://link.aip.org/link/?PHF/14/3046/1>.

[8] H . K . M o att, *Magnetic field generation in electrically conducting fluids* (Cambridge University Press, 1978).

[9] E . C . Bullard and H . G ellman, *Philos. Trans. R . Soc. London, Ser. A* 247, 213 (1954).

[10] A . Reighard and M . Brown, *Phys. Rev. Lett.* 86, 2794 (2001).

[11] E . N . Parker, *Astrophys. J.* 122, 293 (1955).

[12] K . Krause and K . H . R adler, *Magnetohydrody-
namics and Dynamo Theory* (Pergamon Press, 1980).

[13] W . Press, S . Teukolsky, W . Vetterling, and B . F lannery, *Numerical Recipes in C : The Art of Scientific Computing* (Cambridge University Press, 2002), 2nd ed.

[14] E . Spence, C . Forest, M . Norberg, and R . K endrick, (Submitted 2005).

[15] R . H . Kraichnan and S . Nagara jan, *Phys. Fluids* 10, 859 (1967), URL <http://link.aip.org/link/?PZZ/10/859/1>.

[16] N . Pe ey, A . Cawthorne, and D . Lathrop, *Phys. Rev. E* 61, 5287 (2000).